V European Conference on Computational Fluid Dynamics
ECCOMAS CFD 2010
J. C. F. Pereira and A. Sequeira (Eds)
Lisbon, Portugal, 14–17 June 2010

NUMERICAL SIMULATION OF WIND EROSION OF A SINUSOIDAL PILE USING A MOVING BOUNDARY TECHNIQUE

Amir Barati Farimani[*], Almerindo D. Ferreira[†], and Antonio C.M. Sousa[††]

[*†] Universidade de Coimbra, Departamento de Engenharia Mecânica, Pólo II, 3030-788 Coimbra, Portugal

Emails: amir.barati@dem.uc.pt, almerindo.ferreira@dem.uc.pt

[††]University of New Brunswick, Department of Mechanical Eng., P.O. Box 4400, Fredericton N.B., Canada E3B 5A3

Email: asousa@unb.ca

Key words: CFD, wind erosion, pile deformation, saltation, loose boundaries

Abstract. *Prediction of the wind flow over stockpiles and pile formations has the utmost importance in the assessment of potential erosion and evaluation of its environmental impact. The simulation of boundary deformation relies heavily on field experience and, numerical and experimental flow field analyses. In this paper, a computational fluid dynamics approach is used to perform the transient simulation of the boundary deformation of a sand pile. Saltation and creep mechanisms are modeled, and they are considered to be the main erosion mechanisms for the sand transport. The computational predictions are validated against experimental results obtained through wind tunnel tests. The techniques developed and presented allow to evaluate and visualize the erosion on a two dimensional sinusoidal pile, and they contribute to enhanced understanding and prediction of geomorphologic changes.*

1 INTRODUCTION

Fugitive dust emission and undesired geomorphologic changes have driven many researchers to conduct further studies on wind erosion behavior [1-3]. Numerous wind tunnel tests and field observations were carried out to analyze the deformation of stockpiles and sand transport phenomena [4-6]. Interesting qualitative computational models were presented to model snow drift, some of them modeling the erosion, saltation and deposition processes [7-9]. The development of a practical computational erosion simulation paves the way toward the study of the impacts of erosion, estimation of sand transport rate, deposition and surface changes. Computational modeling of erosion additionally provides the opportunity to study the transient nature of erosion in a full scale domain, which is difficult and costly to do experimentally [10]. This modeling is applicable and relevant to many other fields such as moving (loose) boundary, multiphase flow and particle transport [11].

Accurate numerical modeling of surface deformation demands the knowledge of diverse phenomena occurring simultaneously; turbulent flow, erosion, saltation, suspension, creep, and mass flux models need to be considered [12]. Existing analytical models of saltation, creep and erosion can be incorporated into the computational modeling; therefore, when fully calibrated, they greatly contribute to the understanding of the complex nature of erosion [13-15].

In this paper, the computational fluid dynamics (CFD) approach, coupled with a method to model the aeolian erosion is used to simulate simultaneously the wind flow around a dune (pile), and the surface deformation due to sand deposition and erosion. The method incorporates the knowledge of the erosion mechanism, and the commercial CFD code, Fluent 6.3, is used to solve the turbulent flow over the pile [16]; dynamic meshing is enabled to simulate the loose boundary deformations. A User Defined Function (UDF), including dynamic meshing control, erosion, saltation, creep, mass flux, and threshold shear velocity based on variable slope, is coupled to the Fluent code and compiled using Microsoft visual C compiler [17]. Remeshing and smoothing of meshes is performed for each time step. The 2D grid is built in Gambit and exported to Fluent. Modeling of erosion is accomplished by using the threshold shear velocity (u_{*t}) concept. Although there are a few shortcomings for this criterion [18, 19], still is the best known and the best compromise between simplicity and reliability to determine the potential for erosion.

The profile selected in this study, among other possible profiles (e.g. [20, 21]), is one that follows closely a sinus curve; the profile was used for both the experiments and the computational simulations. The pile was exposed to the wind, and its changing profile, due to the erosion, was measured or predicted at specified times.

The method developed in this paper incorporates mass flux conservation. The total sand flux eroded from the surface is assumed to be deposited, saltated or suspended; the consequent deformations of the pile surface are calculated based upon this interchange.

2 COMPUTATIONAL MODEL

In this section of the paper, the computational model and its assumptions and algorithms are explained and discussed.

2.1 UDF algorithm

The computational domain used in this work is assumed to be 2D and it is placed on a plane located midway the length of the pile and normal to its axis. The turbulent fluid field around the pile is solved for each time step. The model assumes unsteady

conditions, and is pressure based; the solver was selected from the computational tool of Fluent [16]. For each time step, the UDF is executed after the required number of iterations to achieve the convergence criterion (maximum residual of 10^{-4}) for each equation is performed. Figure 1 shows the flow diagram of the algorithm used for the UDF; the UDF is assigned only to the pile zone, i.e. the "far-away" region is not considered, as it will be discussed in section 2.2.

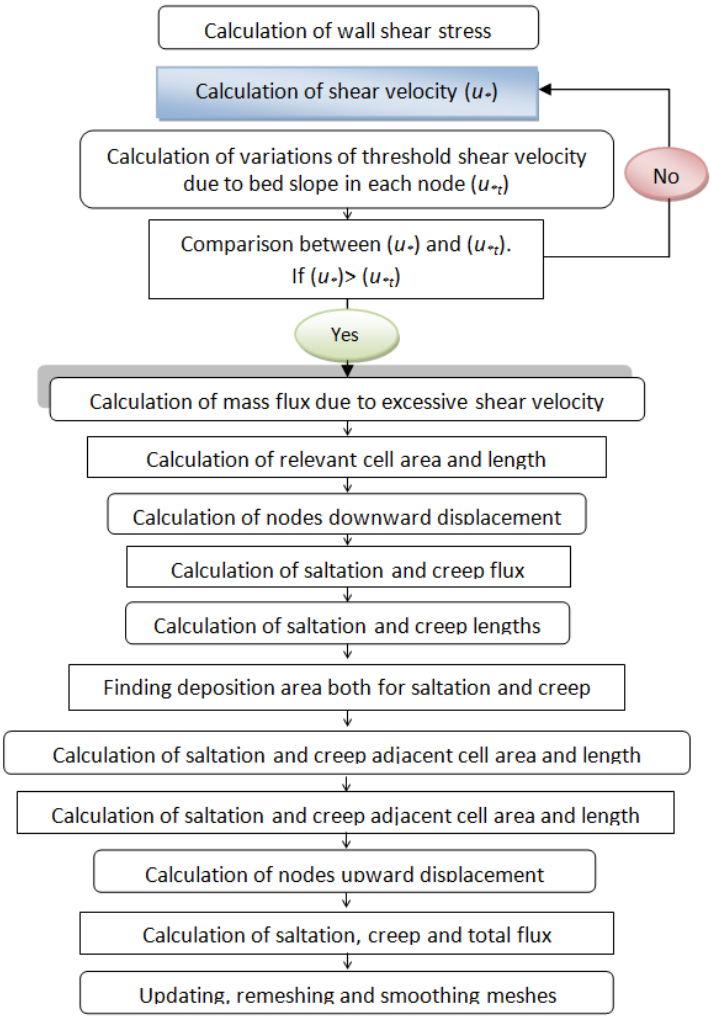

Figure 1: Modeling algorithm.

It should be noted the proposed algorithm can be applied to any type of geometry regardless of its dimensions and shape. The 2D geometry can be placed in any arbitrary position in the computational domain, and the method is totally independent of the meshing.

2.2 Flow simulation and boundary conditions

As already mentioned, the geometry considered has a sinusoidal profile with maximum height (H) of 75 mm and streamwise length (L) of 450 mm ($6H$). The equation of the pile profile and the actual (experimental) cross-section are shown in figure 2.

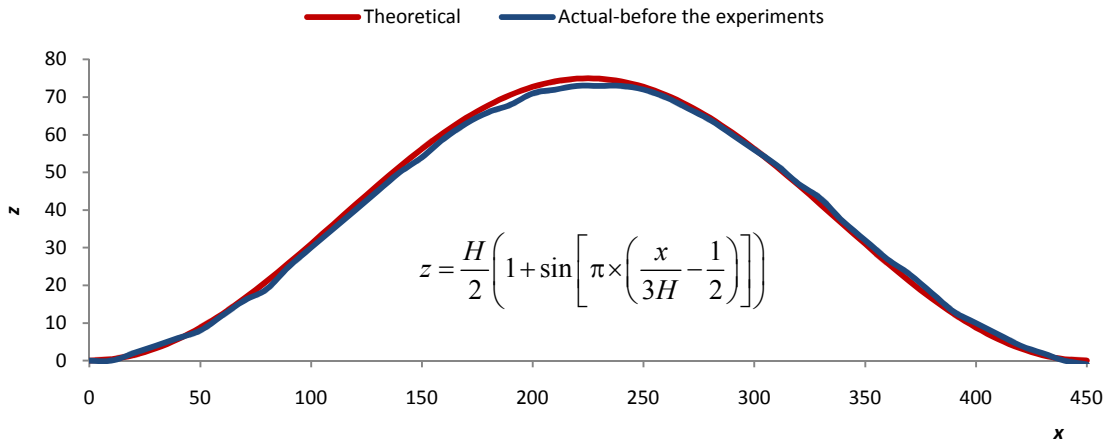

Figure 2: Computational and actual cross-section profiles of the pile.

The computational domain is rectangular with the dimensions indicated in figure 3. To reduce the effect of the inlet and outlet on the flow field, the pile is placed at an extended distance from these boundaries.

The computational domain is taken sufficiently long in the downstream the pile to validate a zero-gradient condition at the outlet. Grid generation is performed by Gambit software [16]. The elements are tetrahedral, and 39423 nodes are generated inside the domain. The pile profile is modeled by 260 nodes distributed along its deformable boundary. The grid and boundary conditions are presented in figure 3.

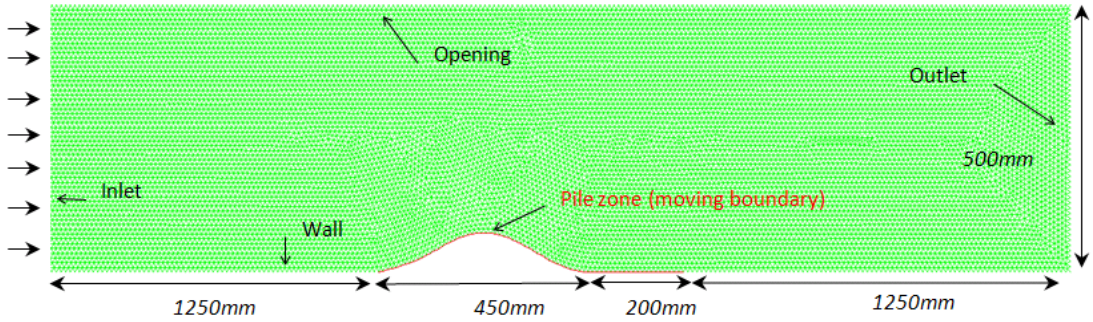

Figure 3: Computational domain including dimensions and boundary conditions.

The fully developed velocity profile, imposed at the inlet boundary, is computed based on the power law profile, namely:

$$\frac{u}{U_0} = (\frac{z}{\delta})^{\alpha} \tag{1}$$

where u is the longitudinal wind velocity component, U_0 is the reference velocity, δ is the boundary layer thickness, the constant α is equal to 0.40 or 0.11, depending on the experimental conditions, and z indicates the vertical height measured from the ground level (wall). The inlet condition, which uses a pre-defined velocity profile, is implemented through a specific UDF [17]. At the outlet boundary, the pressure is set to zero and the pressures calculated within the domain are defined relative to the zero pressure value at the boundary. The upper boundary, named in figure 3 as "opening", is treated as "far field" pressure [16]. The 'no-slip condition' was applied to the fluid–solid interface, and the turbulence is modeled using the standard $\kappa - \varepsilon$ model, which

calculates the turbulent kinetic energy, κ, and its rate of dissipation, ε, based on the assumption the flow is fully turbulent. The magnitude of the molecular viscosity is much smaller than that of the turbulent viscosity; therefore, the molecular viscosity is neglected in this study. The standard wall function is used for the fluid-solid interface; the closure coefficients proposed by Hanjalic and Launder [22] are used for the $\kappa - \varepsilon$ model, and they are: C_μ = 0·09, $C_{\varepsilon 1}$ = 1.44, $C_{\varepsilon 2}$ = 1.92, σ_k = 1.0, σ_ε = 1.30. Wall roughness is set to z_0=0.05 mm, i.e., it is equal to d/10, where d is the grain diameter [23]. Dynamic meshing is assigned to the pile zone (figure 3). Table.1 presents the dynamic meshing values considered in the simulations; the profile is updated at the end of each time step (Δt =1s).

Table 1: Dynamic meshing values [16].

Parameter description	values
Spring constant factor	1
Boundary node relaxation	1
Convergence tolerance	0.001
Minimum length scale	3.348 mm
Maximum length scale	7.783 mm
Maximum cell skewness	0.339

2.3 Variable shear threshold velocity on slope module

There is a considerable body of theoretical work for the threshold shear velocity (u_*) for sand grains spread uniformly over a slope surface. However, if the influence of cohesive forces between particles and the effect of Reynolds number are neglected, then the ratio of threshold on a sloping surface to that on a leveled surface can be given as [24]:

$$\frac{u_{*t}^2}{u_{*t0}^2} = \cos\theta + \frac{\sin\theta}{\tan\alpha} \tag{2}$$

where u_{*t} (m/s) is the local threshold shear velocity on the slope, u_{*t0} is the fluid threshold friction velocity on the leveled surface (without slope), the angle θ is the slope, α is the static friction angle, which is determined from the experimental results of Iversen and Rasmussen [25].

As the profile of the pile is updated for each time step, the angle θ changes, and, consequently, u_{*t} over the pile is computed by the UDF routine. The shear velocity, u_*, is defined as follows:

$$u_* = \sqrt{\frac{2\tau_w}{\rho}} \tag{3}$$

where τ_w is the wall shear stress and ρ the air density.

2.4 Erosion module

As stated in section 2.3, u_{*t} is computed based on the slope. For this calculation the threshold shear velocity value for the flat bed is considered u_{*t0} =0.33 m/s, based on a grain diameter *(d)* of *0.5mm* [11]. For each time step and for each node, the shear velocity is compared to the threshold shear velocity and, if shear velocity for a particular node exceeds the threshold value, then the area (cell) surrounding the node

will be eroded. The corresponding erosion flux, $Q_{erosion}$ (kg/m.s), relative to that node, is calculated based on the relation:

$$Q_{erosion} = C \left(\frac{d}{D}\right)^{0.5} \left(\frac{\rho}{g}\right) {u_*}^3 \tag{4}$$

where D is a standard grain diameter equal to *0.25 mm*, d is the mean grain diameter of the sand for this study (*0.5 mm*), and C is a constant, which may take different values depending on the constitution of the bed (*1.5* for nearly uniform sand, *1.8* for naturally graded sand found on sand dunes, *2.8* for poorly sorted sand with a wide range of grain sizes, and *3.5* for a pebbly surface), and for the present case takes the value of *1.8* [11]. The variables ρ (=1.22 kg/m^3) and g are the air density and the gravity constant, respectively.

The depression of the node satisfying the condition (u_*)> (u_{*t}) and the corresponding area, $h_{erosion}$, caused by the material flux ($Q_{erosion}$) removed from the surface is estimated based on the following relation:

$$h_{erosion} = \left(\frac{Q_{erosion}}{\rho_s . l_n} . \Delta t\right) \tag{5}$$

where ρ_s (=1497 Kg/m^3) is the sand density, l_n is the side length of the cell corresponding to the targeted node, and Δt is the time step. For each time step, the relation is applied to each node to be eroded, and the node is depressed by the corresponding value of $h_{erosion}$.

2.5 Saltation and creep module

A careful review of the literature on saltation and creep related to the dynamics of wind erosion [12, 13] led to the following expression to estimate the saltation flux:

$$Q_{saltation} = C_1 \left(\frac{d}{D}\right)^{0.5} \left(\frac{\rho}{g}\right) u_*^2 (u^* - u_t^*) \tag{6}$$

where C_1 =4.2. The saltation module calculates (u^*, u_t^*) for each time step on the pile zone and its corresponding saltation flux according to equation (6). Considering $Q_{saltation}$ as a packet of sand which is airborne, this packet travels over the pile with two possible paths: it may deposit or a fraction may remain suspended depending on the grain diameter. In the present study, due to the relatively large grain size used (d=0.5 mm), the suspension is low for [26]; therefore, it is neglected. The length, l_{salt}, and the height, h_{salt}, of the grain trajectory (figure 4) are calculated, respectively, by the following relations [13]:

$$h_{salt} = 0.82\, u_*^2 / g \tag{7a}$$

$$l_{salt} = C_s h_{salt} \tag{7b}$$

where the constant C_s may take values between 10 and 15, as reported in [11, 13]. For this study, because there is no prior guidance, a mean value (C_s=12) is selected. The saltation module computes l_{salt} for every node which is targeted based on the value of u^*. The deposition locations are determined by using the relation :

$$Deposition\_Node\_x = Saltation\_Node\_x + l_{salt} \tag{8}$$

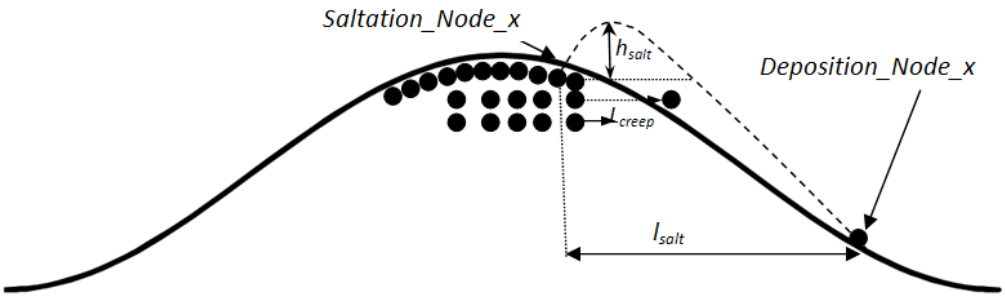

Figure 4: Schematic depiction of saltation and creep.

Deposition_Node_x defines the deposition location for the saltation flux for the pile zone, and *Saltation_Node_x* defines the location from where flux is taken (figure 4). The rise of the deposition node is calculated using the following equation for each time step:

$$h_{Saltation} = \left(\frac{Q_{Saltation}}{\rho_s \cdot l_n}.\Delta t\right) \tag{9}$$

A user subroutine, applying an *ad hoc* algorithm, is used to find the closest node to *Deposition_Node_x* to reduce the computational time. The same procedure is undertaken for creep, whose flux is estimated by the equation:

$$Q_{creep} = \alpha \frac{u_*}{\sqrt{gd}}\, Q_{saltation} \tag{10}$$

where α=0.8 [13].

Unlike the saltation flux, the creep flux is not airborne. The grains roll over the surface based on their initial kinetic energy, which is dissipated through friction and damping on the surface. The average creep length, l_{creep}, is calculated, by considering the friction energy loss and grain kinetic energy, with the following equation [13]:

$$l_{creep} = 0.5\, \frac{u_*^2}{\mu g} \tag{11}$$

where μ is the coefficient of dynamic friction, for which the value of *0.4* was selected, considering sand friction over a sand bed [15]; according to equation (11), those grains with higher velocities roll longer distances on the pile. Creeping deposition locations are estimated based on the following equation:

$$Deposition\_creep\_Node\_x = Saltation\_Node\_x + l_{creep} \tag{12}$$

where *Deposition_creep_Node_x* defines the location on the pile where the creep flux settles; this section of the module estimates the contribution of creep to deposition. It should be noted from equation (10) that creep is represented by a fraction of saltation; ultimately, similarly to the procedure for saltation, the node that receives the material deposition is the one with the closest node coordinates to *Deposition_creep_Node_x* .The vertical rise of the node and corresponding cell, (h_{creep}), due to the material deposition is calculated by the following equation:

$$h_{creep} = \left(\frac{Q_{creep}}{\rho_s . l_n}.\Delta t\right) \tag{13}$$

2.6 Flux module

After the computation of the erosion, saltation and creep fluxes, the UDF module determines the summation of fluxes for each time step. Taking into consideration the

conservation of sand mass, the suspension flux is determined by subtracting to the erosion flux the deposited flux due to saltation and creep, namely:

$$Q_{suspension} = Q_{erosion} - Q_{saltation} - Q_{creep} \quad (14)$$

3 COMPUTATIONAL RESULTS AND DISCUSSION

3.1 Variable threshold shear velocity

As already mentioned, the present approach requires that u_{*t} varies across the pile zone (figure 3), due to the slope variation. The algorithms developed take into account the upslope or downslope conditions. The threshold shear velocity is shown in figure 5, for two time steps; for the first time step, the values of u_{*t} are practically independent from the wind velocity; however, as time goes on, in response to the deformation of the surface due to the wind velocity, changes for, u_{*t} along the surface will occur. The maximum value of u_{*t} occurs on the upslope where θ reaches the higher value. At the initial time (t=0 s) for positions x = 0, 225 and 450 mm, because the surface is horizontal, i.e. there is no slope, the values of u_{*t} approaches the reference value for $u_{*t0}(= 0.33)$ m/s, as proposed by [4]. For t=360s, when the original pile slope has already been considerably deformed, the pile crest region no longer shows the trend originally observed for u_{*t}.

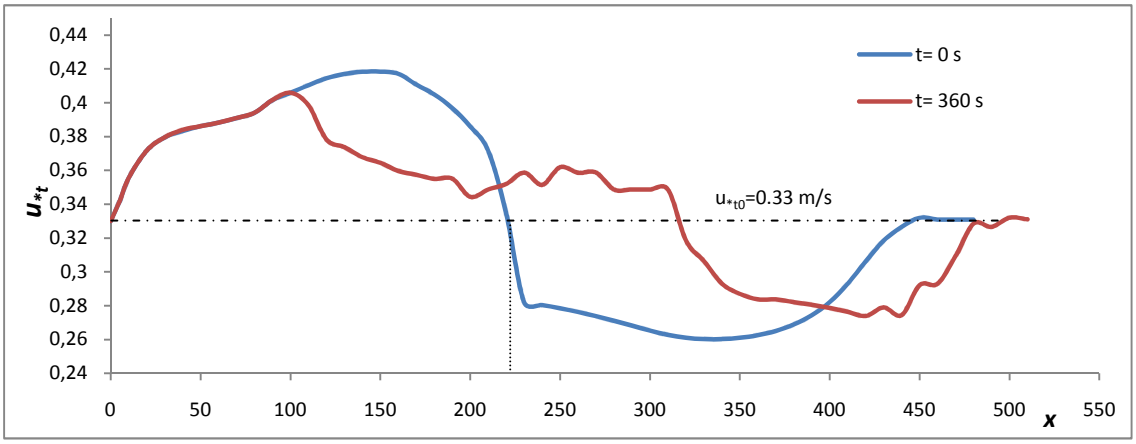

Figure 5: Variation of u_{*t} with time

3.2 Simulation results

For the simulations, an undisturbed wind velocity U_0=8.9 m/s was chosen. Results presented in Figure 6 show the time evolution of the pile as it gets eroded. The erosion process accelerates in the beginning of the simulation because u_* greatly exceeds u_{*t}. The saltation and creep fluxes are transported and deposited mostly on the lee side of the pile and also over the pile extension. Due to the erosion and deposition processes, remeshing and smoothing of the boundary are performed for each time step. Cells with length exceeding the maximum cell length criterion will be subdivided automatically into appropriate triangular elements. The contours of velocity distribution are shown in figure 6; on the lee side, the velocity is quite low, as indicated by the blue color, in comparison with that at the crest region, which is represented in red.

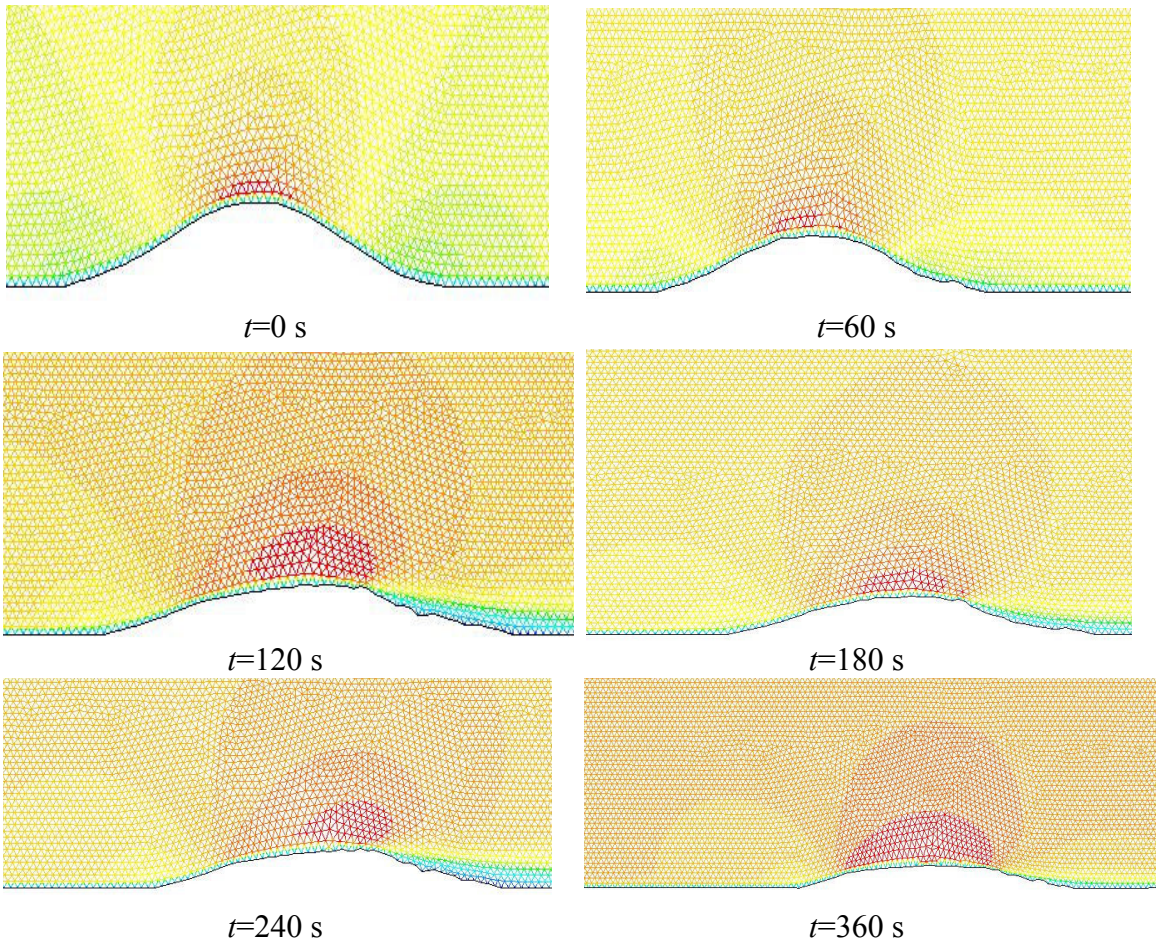

Figure 6: Computational prediction of the pile deformation.

4 VALIDATION

Wind tunnel experiments were conducted to validate the computational results derived from the numerical model. In this section it is described the equipment, the procedure adopted, and the granulometry of the sand used in the experiments.

4.1 Wind tunnel

The wind tunnel used for this study is installed at the Industrial Aerodynamics Laboratory (LAI) of ADAI (Association for the Development of the Industrial Aerodynamics-University of Coimbra, Portugal). This wind tunnel has an open working chamber, which is *5 m* long, placed after a *2 m x 2 m* square cross-section nozzle. The experiment was performed for an undisturbed velocity U_0=*8.9 m/s*. Due to the short length of the working section, no vorticity generators or boundary layer thickness controlling elements were used to change the velocity profile. The profiles of the streamwise velocity component (u) and turbulence intensity are measured at a distance of *2 m* from the nozzle's exit, at half-width of the wind tunnel working chamber; the measured mean velocity profile is consistently correlated by the power law relation expressed by equation (1), which is used in the computational model. The turbulence intensity of the longitudinal velocity component remains nearly unchanged with the height, and it can be taken approximately equal to 15%, as suggested in [26].

The physical model of the dune is a truncated cylinder with a base of sinusoidal profile. It was placed centered on the floor of the working chamber and equidistant to its

sidewalls. The leading edge of the sand was positioned *2.3 m* downstream the nozzle exit, with its axis normal to the main flow direction (figure 7).

Figure 7: Wind tunnel working chamber and pile setup.

4.2 Geometry and pile setup

The experimental pile, as already mentioned, has a sinusoidal profile with maximum height (H) of *75 mm* and streamwise length (L) of *450 mm* ($6H$). The computational equation of the pile profile and the actual cross-section are shown in figure 2. The experimental profile is extruded normal to its plane with a width of *1000 mm* (figure 8). This large length is selected to ensure negligible end effects at the loci placed on the plane normal to the axis of the pile and placed midway the length; this assertion is, in fact, confirmed by the experimental results. Two large Perspex side walls are installed to help reducing the edge effects on the pile (figure 8). For the construction of the dune two wooden guides, with their profile given by the sinus equation (figure2), are placed apart *1000 mm*, and then sieved sand fills the space between them. Then, a ruler supported by the two guides is swept along them for the formation of the sinusoidal pile. This procedure provides for an even and homogenous pile surface. Before the tests, as shown in Figure 2, the surface profile of the pile was measured using a laser device, and good agreement with the sinus equation was observed, as reported in figure 2.

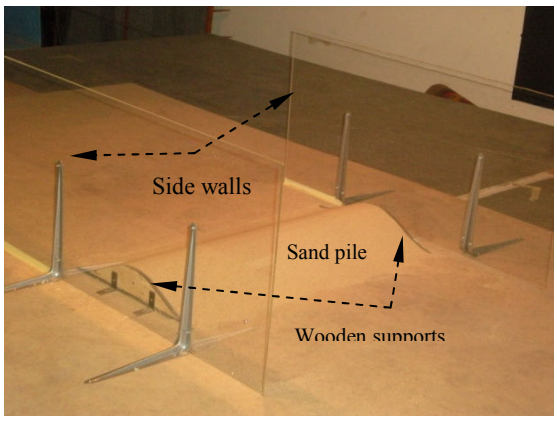

Figure 8: Sand pile prior to the experiments with wooden guides and side walls on each side.

4.3 Sand characterization

For the current experiments, the pile was made out of relatively fine sand. The granulometry test conducted for the sand used revealed the prevailing particles have a diameter of approximately *0.5 mm*, as reported for this type of sand in [26]. The

threshold shear velocity, corresponding to this prevailing particle diameter, is *0.33 m/s*, according to Bagnold's formula [4]. The sand density, measured for this specific granulometry, is equal to 1497 kg/m^3. Prior to the testing, the sand was dried in a furnace during several hours, and then sieved several times to obtain an unconsolidated granular material.

4.4 Test procedure

A laser-based distance measurement instrument (Dimetix, model DLS-B15), placed *2.77 m* above the floor of the working chamber, was used to measure the surface changes of the pile. According with the specifications of the laser instrument, the accuracy of the measurements is *1.5 mm* at a statistical confidence level of 95.4%. The laser is mounted on a traversing system, working on a plane parallel to the base of the model, which allows the laser to be moved in two perpendicular directions. The carrying system is equipped with stepper motors to control the motion and location with high precision. The entire process is computer-controlled, and the distance measurement is processed over the surface profile located half-way the width of the pile. The increment for each successive data point is 5 mm in the streamwise direction. The measurement "sweep" over the profile is conducted sequentially; at each point the distance registered is taken as the average of four laser measurements.

Prior to the start of the data acquisition, the pile was sheltered with a wooden panel until the desired wind velocity was reached; at this point, the protection was removed. At each time step, erosion was allowed during two minutes, after this time the wind tunnel fan is stopped, and the measurement of the profile of the pile is then performed. This routine is repeated after every two minutes of operation.

4.5 Experimental results

Figure 9 shows the time-deformation of the pile, as a consequence of an undisturbed wind velocity of U_0=8.9 m/s. Before starting the erosion, the original pile profile was measured at its centerline, which is shown as the first curve in figure 9. Each measurement "sweep" to register the pile contour is performed after every two minutes (120 seconds). The wind erodes the pile top surface through saltation and creeping processes; this is noticeable from the transition from the second to the third profiles reported in figure 9; there is a shift on the crest area of the pile towards the right. As time advances, the trailing edge of the pile rises. The analysis of the trailing edge is important for a better understanding of the mechanisms involved; therefore, in this study, for each measurement "sweep", the profile of the trailing edge is measured over a region extending *100 mm* beyond the original length of the pile (*L=450 mm*).

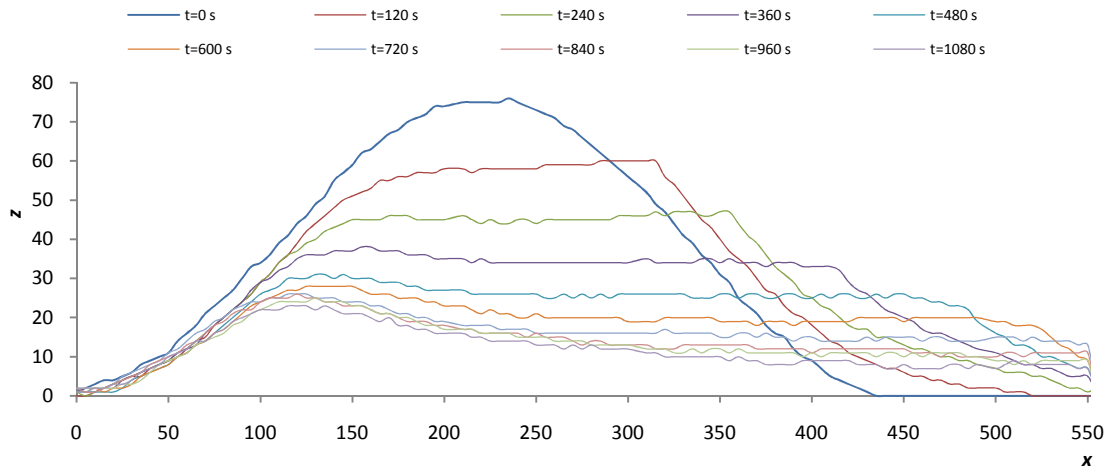

Figure 9: Time-development of the pile profile on a plane normal to the axis and place midway the width for $U_0 = 8.9$ *m/s*.

4.6 Comparison between experimental and computational results

The computational predictions presented in section 3 are compared against the experimental results, which were obtained with identical inlet velocity profiles, as described in section 4.1. Figure 10 shows the comparison between the experimental results and the computational predictions for different time steps. Their agreement, despite a few minor discrepancies, is remarkable. It should be noted that it is critical to take into consideration the dependence of u_{*t} on the local slope .

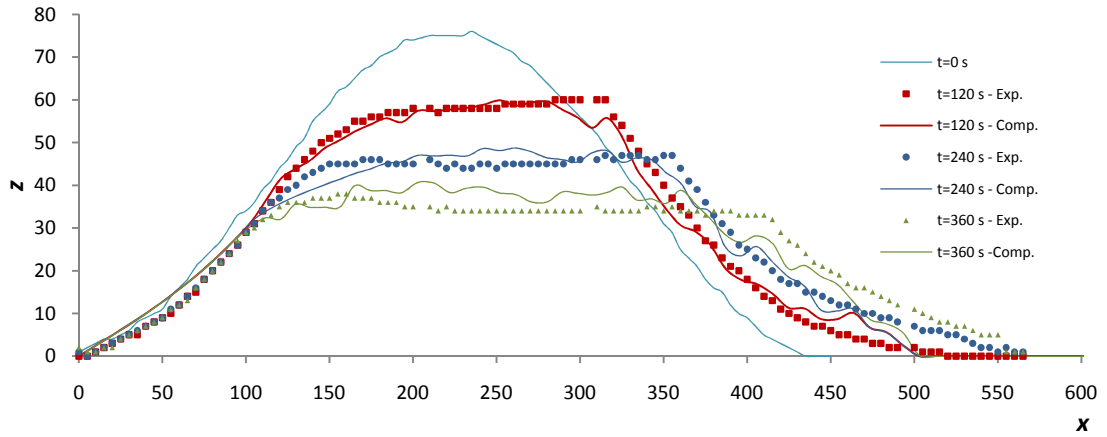

Figure 10: Comparison between the computational predictions and experimental results for the pile profile for different times ($U_0 = 8.9$ m/s).

In what concerns the minor discrepancies and anomalies observed, it is worthwhile to review them as guidance for future developments. The “jumps” that can be noticed in the numerical predictions for the upper part of the pile may be due to excessive accumulation of creep or saltation fluxes. The discrepancies on the lee side and bed extension may be caused by the recirculation zone, which is not fully captured by the computational model. These discrepancies may go back to the creep and saltation models, which incorporate several simplifying assumptions and, in particular the following two: 1. the numerical model considers a uniform sand grain size, while in reality the granulometry tests indicate a broad range of grain sizes; only the prevailing

grain diameter (*d=0.5 mm*) is considered. Models under development are considering the full range of grain sizes, which may affect the value u_{*t0}, and consequently u_{*t}, and the flux models, as expressed by equations (6) and (10); and 2. the present model is applied to conditions, which differ from those used for the derivation of the flux equations; therefore, appropriate calibration tests for the coefficients, such as C_s, α, and μ of equations (7), (9) and (11), are required to guarantee the use of the computational model at its full potential.

5. CONCLUSION

In this study is proposed a computational model for modeling wind erosion deformations, which is applied to the modeling and simulation of the aeolian erosion of a two dimensional sinusoidal sand pile. Analytical models for saltation, creep and mass flux available in the open literature are incorporated in user routines, which are compatible with the CFD software. The overall computational model considers unsteady conditions and it uses a dynamic meshing solver; its main objective is to develop a computational tool, which can predict the erosion and surface deformation of granular material in the form of dunes and stockpiles. Wind tunnel experiments were conducted for a physical model of a dune, and the results were compared against the computational predictions obtained with the computational model developed. The comparison between the experimental results and the computational predictions reveals good agreement. The minor discrepancies may be traced to possible simplifications of the numerical model, in particular, the use of single grain size sand and of constants of the empirical models for erosion, saltation and creep fluxes, which have not been calibrated.

ACKNOWLEDGEMENT

The authors gratefully acknowledge the funding from FEDER and FCT – The Portuguese Foundation for the Science and Technology, through the research project PTDC/EME-MFE/67631/2006, and the doctoral grant SFRH/BD/62519/2009 awarded to ABF.

REFERENCES

[1] EPA, Windbreak coal pile study. Department of Marine, Earth and Atmospheric Sciences, North Carolina State University, *EPA*, **NC 27695-8208** (1985)

[2] EPA, Update of fugitive dust emissions factors in AP-42. Midwest Research Institute, Kansas City, AP-42 section 11.2—*wind erosion*, **MRI No. 8985-K** (1988)

[3] A. Borges and D. Viegas, Shelter effects on a row of coal piles to prevent wind erosion. *J. Wind Eng. Ind. Aerodyn.* **29**, pp.145–154 (1988)

[4] R.A. Bagnold, The Physics of Blown Sand and Desert Dunes. London: *Chapman & Hall* (1941)

[5] Y.H Zhou, X. Guo, and X. J. Zheng, Experimental measurement of wind-sand flux and sand transport for naturally mixed sands, *Phys. Rev. E* **66**, 021305 (20), 9 pages (2002)

[6] R.E. Okoli, Wind tunnel study on aeolian saltation dynamics and mass flow. *J. Arid. Environ.* **53**, pp.569–583 (2003)

[7] J.H.M. Beyers, P.A. Sundsbø and T.M. Harms, Numerical simulation of three-dimensional, transient snow drifting around a cube. *J. Wind Eng. Ind. Aerodyn.* **92**, pp.725–747 (2004)

[8] Moore, I., Numerical modeling of blowing snow around buildings. Ph.D. Dissertation, *Department of Applied Mathematical Studies*, University of Leeds (1995)

[9] J. Lays, G. M. Tanish and Y. Shao, Wind erosion monitoring and modeling technique in Australia, *D.E Stott, R.H. Mohtar and G.C Steinhardt (eds)*, *Sustaining the global Farm* (2001)

[10] Q. Sun, G. Wang and Y.Xu, DEM Applications to aeolian sediment transport and impact process in saltation. *Part. Sci. Technol.* **19**, pp.339-353 (2001)

[11] K.Pye. and H. Tsoar, Aeolian Sand and Sand Dunes. *Unwin Hyman*, London (1990)

[12] Z.T. Wang and X.J Zheng, Theoretical prediction of creep flux in aeolian sand transport, *Powder Technol.* **139** , pp.123– 128 (2004)

[13] B. Andreotti, P. Claudin and S. Douady, Selection of dune shapes and velocities. Part 1: Dynamics of sand, wind and barchans. *Eur. Phys. J. B* **28**, pp.321– 341 (2002)

[14] R.S. Anderson, M. Sorensen and B.B. Willetts, A review of recent progress in our understanding of aeolian sediment transport. *Acta Mech.*, **Suppl. 1**, pp. 1–19 (1991)

[15] Y. Shao, Physics and Modeling of Wind Erosion*, Kluwer Academic Publishing*, Dordrecht (2000)

[16] FLUENT, FLUENT User's guide V6.3, *Ansys Fluent Inc.* (2006)

[17] FLUENT.FLUENT UDF manual V.6.3, *Ansys Fluent Inc*. (2006)

[18] J.H.M. Beyers, Numerical modeling of the snowdrift characteristics surrounding the SANAE IV research station, Antarctica. Ph.D. Dissertation, *Department of Mechanical Engineering, University of Stellenbosch*, Stellenbosch, South Africa. (2004a)

[19] J.H.M. Beyers, Numerical simulation and verification of drifting snow around a cube. *J. Wind Eng. Ind. Aerodyn*. **92**, pp.725–747 (2004b)

[20] T. Badr and J.L. Harion, Effect of aggregate storage piles configuration on dust emissions. *Atmos. Environ*. **41**, pp.360-368 (2007)

[21] J.A. Toraño, R. Rodriguez, I. Diego, J.M. Rivas and A. Pelegry, Influence of the pile shape on wind erosion CFD emission simulation. *Appl. Math Model* **31**, pp.2487–2502 (2007)

[22] K. Hanjalic and B.E. Launder, A Reynolds stress model of turbulence and its application to thin shear flows. *J. Fluid Mech*. **52**, pp.609–638 (1972)

[23] N. Lancaster, Geomorphology of Desert Dunes. London, Routledge, 244 pp. (1995)

[24] N. Huang, F. Shi and R. Scott Van Pelt, The effects of slope and slope position on local and upstream fluid threshold friction velocities. *Earth Surf. Processes Landforms* **33**, pp.1814–1823 (2008)

[25] J.D. Iversen and K.R. Rasmussen, The effect of surface on saltation threshold. *Sedimentology* **41,** pp.721–728 (1994)

[26] A.D. Ferreira and R.A. Oliveira, Wind erosion of sand placed inside a rectangular box. *J. Wind Eng. Ind. Aerodyn*. **97,** pp.1–10 (2009)